PHILOSOPHICAL MAGAZINE A, 2001, VOL. 81, NO. 9, 2243–2269

Grain-boundary migration in the presence of diffusing impurities: simulations and analytical models

M. I. MENDELEV, D. J. SROLOVITZ†

Princeton Materials Institute and Department of Mechanical and Aerospace Engineering, Princeton University, Princeton, New Jersey 08544, USA

and W. E

Program in Applied and Computational Mathematics and Mathematics Department, Princeton University, Princeton, New Jersey 08544, USA

[*Received 19 June 2000 and accepted in revised form 5 December 2000*]

ABSTRACT

The mobilities of grain boundaries is a key factor in determining the evolution of polycrystalline microstructures. In most cases, the intrinsic boundary mobility is strongly affected by the presence of impurities. We present a series of simulations of grain-boundary migration in systems without impurities, with static impurities and with impurities that are free to diffuse. The simulations are performed within a kinetic Monte Carlo formalism based upon a simple spin model with interstitial impurities and consider the effects of bulk impurity concentration, impurity diffusivity, interaction strength and temperature. Two regimes of motion were distinguished (at low and high velocities) with a smooth transition between them under all conditions. Contrary to the classical continuum model of impurity drag, the simulation results demonstrate that attractive and repulsive impurity–grain-boundary interactions yield very different grain-boundary mobilities and the domain wall velocity never exhibits sharp jumps. A discrete model is developed that properly describes the transition between regimes and the differences between attractive and repulsive impurities.

§1. INTRODUCTION

The fundamental mechanisms by which extended defects move in solids have been of widespread interest since the inception of the science of materials as a discipline. Although the detailed atomistic mechanisms associated with this type of motion are generally unknown (for example Gottstein and Shvindlerman (1999)), it is possible to analyse several important aspects of this motion without such information. These include a general rate theory description of migration and a description of the motion of extended defects in crystalline materials in terms of nucleation and propagation of kinks. For a description of the rate theory approach, see Mott (1948), Hirth and Lothe (1982), Sutton and Balluffi (1995) and Gottstein and Shvindlerman (1999). It is widely accepted that extended defects such as dislocations and grain boundaries move by the formation and migration of kinks and islands or steps, for

† Email: srol@princeton.edu

Philosophical Magazine A ISSN 0141–8610 print/ISSN 1460-6992 online © 2001 Taylor & Francis Ltd
http://www.tandf.co.uk/journals
DOI: 10.1080/01418610010029007

one-dimensional and two-dimensional defects respectively (Sutton and Balluffi 1995, Gottstein and Shvindlerman 1999). The rates of double-kink and/or double island nucleation and how quickly kinks and steps move depend on such factors as the sharpness of the kinks, the kink heights and the number of atoms involved in the unit step of kink motion. Nonetheless, many features of the intrinsic motion of such extended defects can be determined by investigations based on generic models that incorporate kink nucleation and motion. In our earlier work (Mendelev and Srolovitz 2000a), we considered how the velocity of an extended defect depends on the driving force and the temperature. An analytical expression was obtained in those studies and was successfully compared with results of Monte Carlo simulation. In the present work, we examine the influence of diffusing impurities on boundary migration.

It is well known that even a very small concentration of impurities can greatly modify grain boundary migration rates, as noted in recrystallization and grain growth experiments. Therefore, it is important to develop a quantitative understanding of the relationship between grain-boundary velocity and the driving force for boundary migration in the presence of impurities. The first quantitative analysis of this problem was suggested by Lücke and Detert (1957). In this analysis, the concentration of the impurities near a flat boundary was described using Boltzmann statistics:

$$C_0 = C_\infty \exp(-E/kT), \tag{1}$$

where C_∞ is the impurity concentration (atomic fraction) away from the boundary (i.e. the mean impurity concentration), kT is the thermal energy and E is the boundary–impurity interaction energy. The force exerted on the boundary by the impurity atoms is written as

$$P_\mathrm{i} = nC_0 f, \tag{2}$$

where n is the number of impurity atoms per unit area of the boundary and f is the force exerted on the boundary by one impurity. In the steady state, the boundary moves with constant velocity V, which is related to the impurity drag force via the Einstein relation (Lücke and Detert 1957) as

$$V = \frac{D}{kT} f, \tag{3}$$

where D is the impurity diffusivity. Combining equations (1)–(3) yields

$$V = \frac{D}{kT} \frac{1}{nC_\infty \exp(-E/kT)} P_\mathrm{i}. \tag{4}$$

A serious flaw in this analysis is associated with the fact that equation (1) is only valid in the limit of zero boundary velocity. To correct this deficiency, Cahn (1962) analysed the impurity flux J to give

$$J = -\frac{DC}{kT}\frac{\mathrm{d}\mu}{\mathrm{d}x} - VC = -D\frac{\mathrm{d}C}{\mathrm{d}x} - \frac{DC}{kT}\frac{\mathrm{d}E}{\mathrm{d}x} - VC, \tag{5}$$

where μ is the impurity chemical potential and the boundary–impurity interaction energy $E(x)$ is an explicit function of the separation x between the boundary and an impurity. If $V = 0$, then $J = 0$ and equation (5) reduces to equation (1). In the steady state, $J = -VC_\infty$ and equation (5) reduces to

$$D\frac{\mathrm{d}C}{\mathrm{d}x}+\frac{DC}{kT}\frac{\mathrm{d}E}{\mathrm{d}x}+VC=VC_{\infty}. \tag{6}$$

Cahn (1962) gave a general integral expression for the steady-state impurity concentration profile. This equation was explicitly solved for the case of a triangular boundary–impurity interaction profile.

The drag force associated with any interaction profile can be obtained as

$$P_{\mathrm{i}}=-n\int_{-\infty}^{+\infty}C(x)\frac{\mathrm{d}E}{\mathrm{d}x}\,\mathrm{d}x. \tag{7}$$

In the steady state, the driving force is equal to (Cahn 1962)

$$P=P_0(V)+P_{\mathrm{i}}(V,C_{\infty}), \tag{8}$$

where $P_0(V)$ is the intrinsic force–velocity relation associated with boundary migration in the impurity-free material. The resultant force–velocity relation suggests the existence of two types of behaviour, depending on conditions:

(i) a monotonic nonlinear relation;
(ii) a relation in which the boundary velocity exhibits a discontinuous jump at a particular driving force.

We return to these classical results when we analyse the data from the simulations presented herein.

While Cahn's (1962) analysis corrected important deficiencies in the work of Lücke and Detert (1957), it too has several problems.

(i) It assumes that the boundary remains flat as it migrates (i.e. the infinite surface tension limit), while in real systems the boundary is generally not flat. Modern atomic theories of boundary migration show that boundaries move by kink formation and migration, resulting in non-flat boundaries and nonlinear force–velocity relations.
(ii) Because boundaries move by kink formation and migration, a complete model of boundary migration must account for the fact that the kink formation and migration energies are modified by interactions with impurities, suggesting that equation (8) is an oversimplification.
(iii) The second equality in equation (5) is based on the simplifying assumption that the system is an ideal solution. Recent work (Mendelev and Srolovitz 2000b) has shown that the assumption of ideality can lead to mobilities that are in error by several orders of magnitude in some cases where the impurities are attracted to the boundary.
(iv) Equation (1) is not valid when the impurity–boundary interaction is strongly attractive or the bulk impurity concentration is large, since the concentration at any point in the material must always be less than or equal to unity. For a typical interaction strength $E(0)=-0.13\,\mathrm{eV}$ (Lücke and Detert 1957), the concentration at the boundary at room temperature (according to equation (1)) is 152 times greater than the bulk concentration. For a bulk solute concentration of only 0.66%, the concentration at the boundary exceeds one. Thus, any approach that does not account for site saturation even in ideal solutions (such as that suggested by Cahn (1962)) is of limited applicability. Lücke and Stüwe (1963), considering site saturation, rewrote equation (5) as

$$D\frac{dC}{dx}+\frac{D}{kT}C(1-C)\frac{dE}{dx}+VC=VC_{\infty}. \quad (9)$$

For $V=0$, this equation yields the classical result:

$$C=\frac{C_{\infty}\exp[-E(x)/kT]}{1-C_{\infty}+C_{\infty}\exp[-E(x)/kT]}. \quad (10)$$

While this equation is valid for ideal solutions at any concentration, Lücke and Stüwe only considered $V\neq 0$ for the case in which the mean concentration was small, that is equation (5).

(v) Since the range of the impurity–boundary interaction is typically considered to be very small (no more than a few interatomic spacings), it is unclear whether it is appropriate to describe impurity diffusion using a continuum equation. To address this issue, Lücke and Stüwe (1963) suggested a discrete model to describe impurity diffusion with both one- and two-dimensional features.

(vi) Finally, we note that the functions $E(x)$ and $D(x)$ are generally unknown in the vicinity of the boundary, making direct comparisons between experiment and theory nearly impossible.

Several other analyses of this problem have been presented in the literature. For example, the influence of the impurities on boundary mobility may be associated with the difference in atomic mobilities of matrix and impurity atoms across the boundary (Westengen and Ryum 1978) . More complete reviews of the influence of impurities on boundary migration may be found in the paper by Hillert (1999).

Since all the existing theoretical analyses of the effects of diffusing impurities on boundary migration make one or more of these limiting assumptions in order to keep the problem tractable, these theories have had limited success in explaining the experimental observations. In the present work, we relax a number of these assumptions within the framework of a computer simulation. The simulations are performed within the framework of a simple model, which is an extension of the well known Ising model. The results are compared directly with theoretical predictions and extensions to existing theory are proposed.

§2. Simulation method

The simulations are performed using a two-dimensional Ising model, such that the grain boundary is a line. The driving force for boundary migration is an applied field, akin to that used in experiments on magnetically anisotropic materials (Molodov *et al.* 1999). In this framework, the bicrystal is replaced by a regular (square) lattice of spacing a, each occupied by a 'spin' that identifies the crystal orientation. Since we focus on a bicrystal, we consider only up and down spins, $s_i=\pm 1$, where i identifies the site. In this picture, a grain boundary is located between spins of opposite orientation (figure 1). The temporal evolution of the model is stochastic and simulated via the Monte Carlo method with spin-flip dynamics (i.e. Glauber dynamics). A rectangular simulation cell is employed, with toroidal boundary conditions, that is periodic along the top and bottom surfaces and inverse periodic boundary conditions along the left and right surfaces (i.e. $s_i\rightarrow -s_i$ on crossing these surfaces). This boundary condition is employed to ensure that the system contains only one grain boundary. The numbers of atomic sites along the x and y directions are n_x and n_y respectively. The impurity (solute) atoms sit exclu-

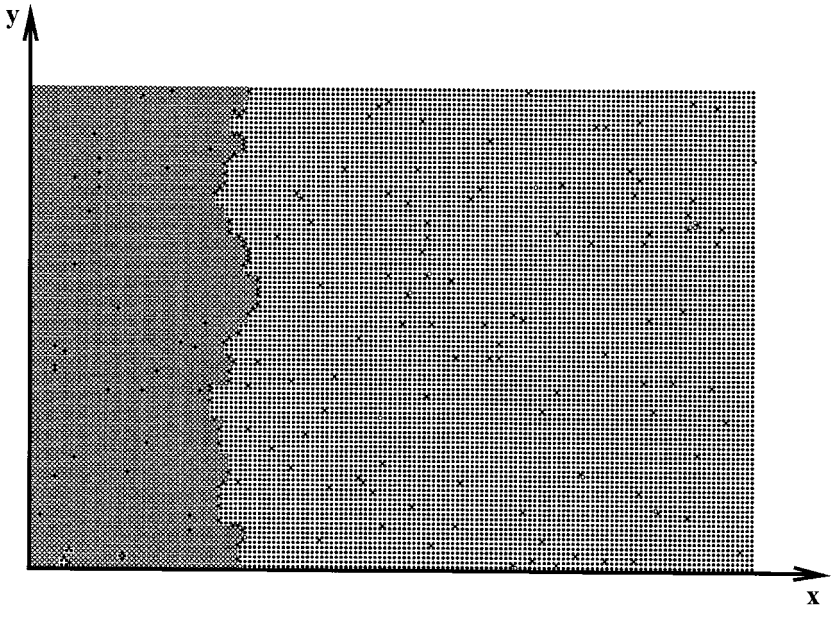

Figure 1. Illustration of simulation model. The full and open circles refer to $s_i = +1$ and $s_i = -1$, respectively. The boundary is the junction of the full and open circles. The small full square in the interstices of the regular lattice indicates the location of impurities.

sively on interstitial sites (see figure 1). The initial locations of the impurity atoms are assigned at random and C_∞ is the fraction of atoms that are impurities: $C_\infty = N_\mathrm{i}/(N_\mathrm{s} + N_\mathrm{i})$, where N_i is the number of impurities and $N_\mathrm{s} = n_x n_y$.

In the absence of impurities, the total energy of the system is

$$E^{\mathrm{ss}} = -\frac{J}{2}\sum_{\langle i,j\rangle} s_i s_j - H\sum_i s_i, \tag{11}$$

where H is the field that drives the boundary motion and J is a constant that is proportional to the boundary energy (per lattice spacing in two dimensions). In the normal magnetic language of Ising models, H is a magnetic field, J is the exchange integral and s_i is the dipole moment associated with the spin on site i. The first summation in equation (11) is over all sites i and their four nearest neighbours j. The system was initialized with all the sites in the right half of the cell with $s_i = +1$ and those in the left half of the cell with $s_i = -1$.

In the presence of impurities, the total energy of the system can be written as

$$E = E^{\mathrm{ss}} + E^{\mathrm{si}} + E^{\mathrm{ii}}, \tag{12}$$

where the second term is the interaction energy between the solvent and impurity atoms and the last term is the impurity–impurity interaction energy. In the present work,

$$E^{\mathrm{si}} = -\frac{E_0}{4}\sum_i \left|\sum_j s_j\right|, \tag{13}$$

where the first sum is over all impurity atoms and the second sum is over nearest neighbours of impurity i. We investigated both cases corresponding to attractive ($E_0 < 0$) and repulsive ($E_0 > 0$) impurity–boundary interactions. The impurity–impurity interaction energy is described by

$$E^{ii} = \phi \sum_{\langle i,j \rangle} \theta_i \theta_j, \tag{14}$$

where the summations are over all impurity sites and their nearest-neighbour impurity sites $\theta_i = 1$ or 0 if impurity site i is occupied or empty respectively. In the present simulation, we choose $\phi \geqslant 0$ to ensure that the impurities do not form precipitates.

The following algorithm is employed to describe the evolution of the model. We first generate a random number R_1 (all random numbers used throughout are uniform deviates in the range $0 < R \leqslant 1$). If $R_1 \geqslant C_\infty$, then a solvent atom is considered. This solvent atom is chosen at random and an attempt is made to flip its sign (i.e. $s_i \rightarrow -s_i$). If the energy change associated with this flip does not raise the energy, $\Delta E \leqslant 0$, this spin flip is accepted. If $\Delta E > 0$, a random number R_2 is generated. If $R_2 < \exp(-\Delta E/kT)$, this spin flip is accepted; otherwise the spin is returned to its original orientation (kT is the thermal energy). If $R_1 < C_\infty$, another random number R_3 is generated and compared with the relative impurity mobility M (M is equal to four times the impurity diffusivity D). If $R_3 \leqslant M$, then an impurity and a direction of motion are chosen at random (from among the four nearest-neighbour impurity sites; impurities are not allowed to cross the left and right edges of the simulation cell). If the new site is empty ($\theta_i = 0$) and $\Delta E \leqslant 0$ this movement is accepted. If $\Delta E > 0$ and $R_4 < \exp(-\Delta E/kT)$, this movement is accepted; otherwise it is rejected. In the present simulations, time is directly proportional to the number of site exchange or reorientation attempts. We define the time associated with the attempt to flip each site once, on average, as our unit of time: 1 Monte Carlo step (MCS) site^{-1}.

The mean boundary position p was determined by summing the values of all the regular site occupancies (i.e. determining the total magnetization):

$$p = \frac{n_x}{2}\left(1 - \frac{1}{n_x n_y}\sum_i s_i\right). \tag{15}$$

With $H > 0$, the boundary moves to the left. In order to prevent the boundary from running to the edge of the simulation cell, we employed the following algorithm. When the boundary translated to within $n_x/4$ of the left edge of the simulation cell, a section of the simulation cell of size $n_x n_y/4$ is removed from the right side of the model and a section of the same size is added to the left side. This allows the boundary to keep moving rather than hitting the edge of the model. The impurity concentration in the added part is C_∞. This approach corresponds to the view that the boundary is always moving into pristine material (a grand canonical ensemble).

§ 3. Simulation results

Several series of simulations (figure 1) were performed over a range of driving forces H for different values of the materials parameters: impurity diffusivity D, impurity–boundary interaction strength E_0, impurity–impurity interaction strength ϕ and bulk impurity concentration C_∞. In addition, we investigated the effects of changing the temperature T. A list of the cases examined may be found in table 1.

Table 1. List of parameters for which simulations were performed.

Series	E_0 (J)	D (a^2 (MCS site^{-1})$^{-1}$)	T (J/k)	C_∞	ϕ (J)
1	−3.26	0.091 6	0.5	0.010	1
2	−3.26	0.022 9	0.5	0.010	1
3	−3.26	0.000 0	0.5	0.010	1
4	−1.63	0.091 6	0.5	0.010	1
5	1.63	0.091 6	0.5	0.010	1
6	3.26	0.091 6	0.5	0.010	1
7	−1.63	0.091 6	0.25	0.010	1
8	1.63	0.091 6	0.25	0.010	1
9	−1.63	0.001 68	0.25	0.010	1
10	1.63	0.001 68	0.25	0.010	1
11	1.63	0.001 68	0.25	0.010	0
12	1.63	0.001 68	0.25	0.010	0
13	−3.26	0.022 9	0.5	0.001	1
14	3.26	0.022 9	0.5	0.001	1
15	3.26	0.091 6	0.5	0.005	1
16	3.26	0.091 6	0.5	0.005	1
17	3.26	0.000 0	0.5	0.010	1

The results of simulations performed for the special case of no impurities were reported earlier (Mendelev and Srolovitz 2000a).

In the first series of simulations, labelled series 1 in table 1, we consider the case of impurities that are attracted to the interface ($E_0 < 0$). The upper limit on the driving force H was chosen to ensure that no new domains were nucleated by thermal fluctuations away from the boundary during the course of the simulation. Figure 2 shows the configuration of the model at an arbitrary (long) time for two different values of the driving force ($H = 0.01$ and 0.10). Figure 3 shows the configuration of the system at several times for an intermediate value of the driving force ($H = 0.045$). Clearly, at small H, the impurities strongly segregate to the migrating boundary. However, at large H, the degree of segregation is small. For intermediate H, there are sections of the boundary where segregation is large and sections where it is small (see the circled region in figure 3 (*b*)).

Each simulation for a particular set of parameters yields a plot of the boundary position versus time, as shown in figure 4 for the same conditions as in figures 2 and 3. Clearly the boundary moves more rapidly with increasing driving force. The displacement–driving force relation is nearly linear in the absence of impurities (Mendelev and Srolovitz 2000a). Similarly, when the driving force is large, the displacement–driving force relation is also linear (figure 4 (*c*)). At small driving force, the displacement–driving force relation is linear after an initial transient stage (of approximate duration 10^5 MCS site^{-1} in figure 4 (*a*)). During the transient regime (not shown), the boundary collects more impurity atoms while it migrates, leading to a decreasing velocity. In the late-time regime, the impurity concentration on the boundary becomes time independent. In this state, the impurity concentration on the boundary is high. In this late-time regime, a steady state is established between impurities becoming attached to the boundary and impurities falling off the boundary. This stochastic dynamic process leads to the high-frequency variation in boundary position with time, which would not be seen in a much larger model.

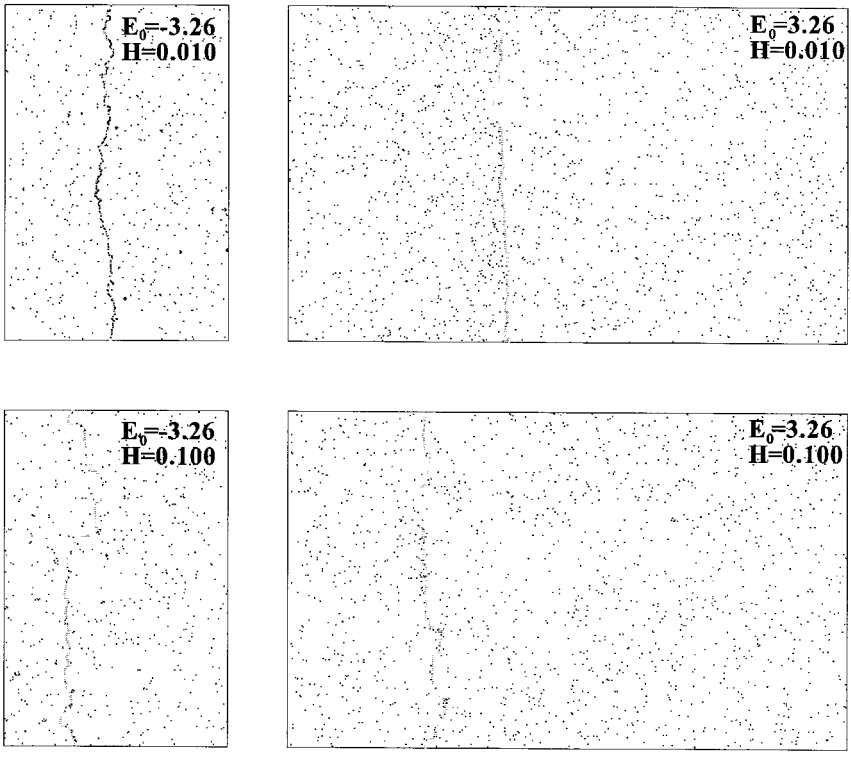

Figure 2. Images from simulations showing the position and shape of the boundary (light-grey line) and the impurities for two different values of the driving force and opposite signs of the interaction strength (indicated in the upper right corner of image). These simulations were all performed using $C_\infty = 0.01, D = 0.0916a^2\,(\mathrm{MCS\,site}^{-1})^{-1}$ and $T = 0.5\,\mathrm{J}/k$.

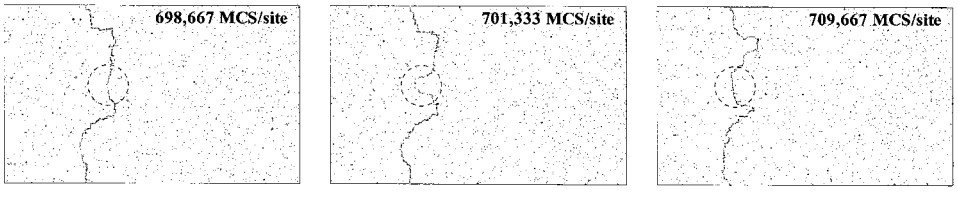

Figure 3. Images from simulations performed using $H = 0.045$, $E_0 = -3.26$, $C_\infty = 0.01$, $D = 0.0916a^2\,(\mathrm{MCS\,site}^{-1})^{-1}$ and $T = 0.5\,\mathrm{J}/k$ three times. The broken circle indicates the position where there is a bulge in the boundary.

In the intermediate-driving-force case, some sections of the boundary manage to break away from the impurities in regions where the local impurity concentration is (stochastically) low. This is shown clearly in figure 3, where such a low-impurity-concentration section of the boundary bulges out, moving rapidly ahead of the rest of the boundary, followed by the lateral motion of the sides of the bulged region. Further advancement of the bulged region ahead of the rest of the boundary is restricted by the surface tension of the boundary and further adsorption of impurities atoms on the leading edge of the bulge. This type of motion gives rise to the low-frequency noise in the displacement–driving force relation shown in figure 4 (*b*).

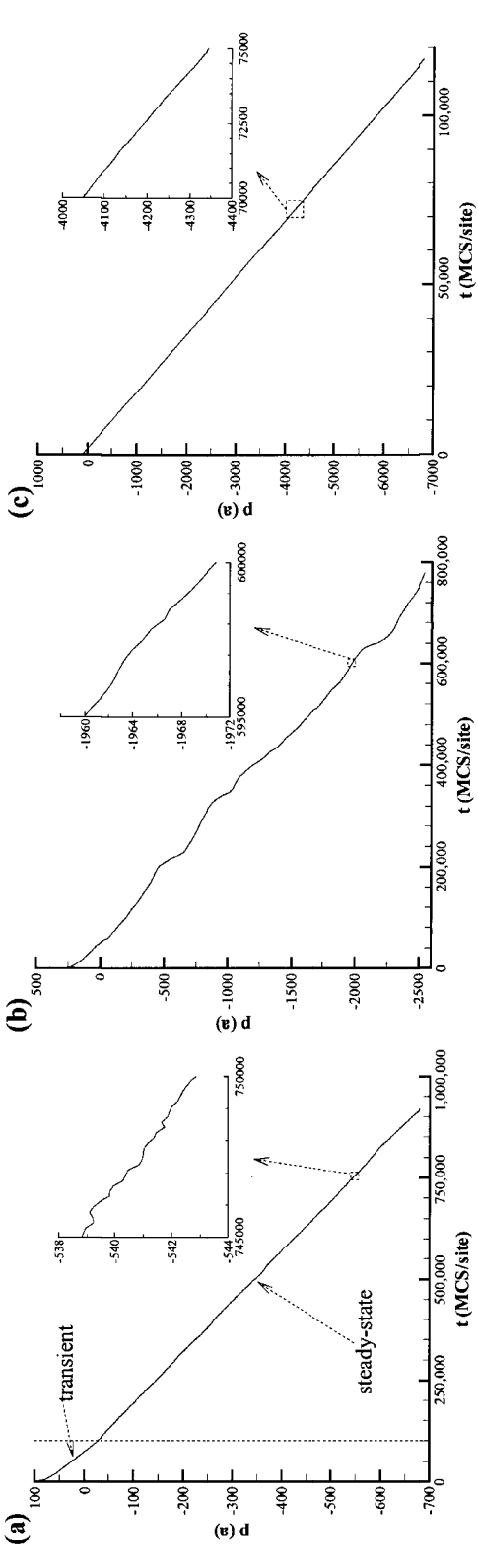

Figure 4. The time dependence of the mean boundary position in simulations performed at three driving forces (*a*) $H = 0.030$, (*b*) $H = 0.045$ and (*c*) $H = 0.100$ in simulations performed using $E_0 = -3.26$, $C_\infty = 0.01$, $D = 0.0916a^2$ (MCS site^{-1})$^{-1}$ and $T = 0.5$ J/k. The insets show enlarged portions of the main plots.

Comparison of the boundary shapes at small (figure 2 (*a*)), intermediate (figure 3) and large (figure 2 (*b*)) driving forces shows that the boundary is considerably rougher at intermediate driving forces. This is clearly related to this boundary bulging phenomenon described above, which does not occur at either large or small driving forces. This observation is quantified in figure 5 (*a*) where we examine the roughness, as measured by the excess boundary length $L/n_y - 1$, as a function of the driving force. For the case of impurities attracted to the grain boundary ($E_0 < 0$), the boundary roughness is nearly constant at small driving forces, increases abruptly at intermediate driving forces and then decays at large driving forces. The magnitude of the peak in the roughness (figure 5 (*a*)) should be viewed as a lower bound on the true roughness, because the magnitude of the roughness at intermediate driving forces (only) increased with simulation cell size.

Since this bulging phenomenon is related to the impurity concentration on the boundary, we also examine how the fraction (X_0) of boundary sites occupied by impurities varies with the driving force (figure 5 (*b*)). At both small and large driving forces, the concentration of impurities on the boundary varies only weakly with the driving force. At small driving forces, this can be attributed to the fact that the impurities have little difficulty keeping up with the slow moving boundary and are essentially in equilibrium with the boundary (i.e. this is the quasistatic boundary limit; see below). At large driving forces, the impurities have insufficient time to move in response to the presence of the fast-moving boundary, that is the quasistatic impurity limit. This is supported by the observation that the impurity concentration on the boundary in the present finite-diffusivity case approaches the results for the limiting case of zero impurity diffusivity (see figure 5 (*b*)). There is a smooth transition between the high impurity concentrations on the boundary at small driving forces and the low impurity concentrations on the boundary at large driving forces that begins at approximately the same driving force where the roughness rapidly increases (cf. figures 5 (*a*) and (*b*)).

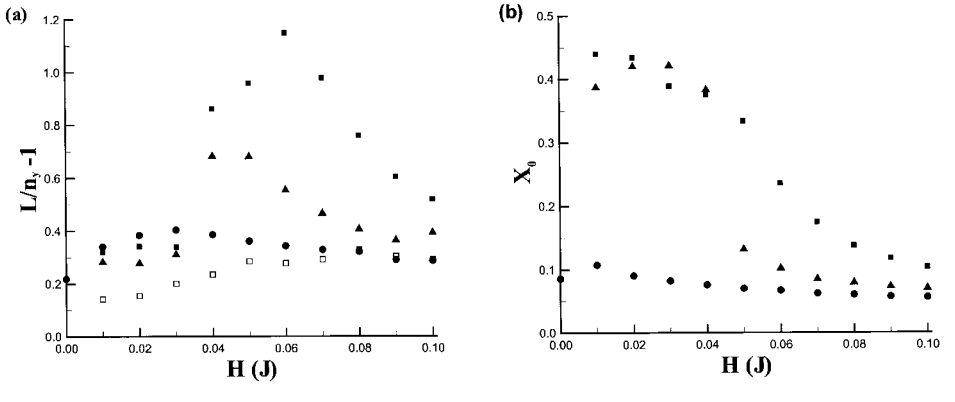

Figure 5. (*a*) The boundary roughness (i.e. normalized excess length) versus the driving force. (*b*) The impurity concentration at the boundary versus the driving force. The simulations were performed using $C_\infty = 0.01$ and $T = 0.5\,\mathrm{J}/k$ for three different diffusivities ((●), $D = 0$; (▲), $D = 0.0229a^2\,(\mathrm{MCS\,site}^{-1})^{-1}$; (■), (□), $D = 0.0916a^2\,(\mathrm{MCS\,site}^{-1})^{-1}$) and two different signs of the interaction strength ((●), (▲), (■), $E_0 = -3.26\,\mathrm{J}$; (□), $E_0 = +3.26\,\mathrm{J}$).

The dependence of the boundary velocity V (i.e. the mean slope obtained at late times from figure 4 and similar plots) on the driving force is shown in figure 6. In the present case ($E_0 = -3.26$; $D = 0.0916$), the boundary velocity increases linearly, but slowly, with increasing driving force for small H. The velocities are all reported in units of $v = a\,(\mathrm{MCS\,site^{-1}})^{-1}$. At large driving forces, the velocity is also approximately a linear function of the driving force, although with a considerably larger slope. These two observations support the notion of two distinct boundary migration regimes. Comparing figure 6 with figure 5 (*a*) shows that the transition between these two regimes occurs near the same driving force where the roughness rapidly increases and where the impurity concentration on the boundary decreases.

We performed two series of simulations designed to investigate the influence of impurity diffusivity on boundary velocity: series 2 with $D = 0.0229$ and series 3 with $D = 0$ and all other parameters unchanged (see table 1). The data for these two series are also shown in figures 5 and 6. These figures demonstrate that decreasing the impurity diffusivity decreases the concentration of impurities on the boundary, decreases the boundary roughness and decreases the driving force at which the transition between the low- and high-boundary-mobility regimes occur. Decreasing the diffusivity to zero fundamentally changes the behaviour of the system, because the pinned boundary can move only by thermal excitation off the

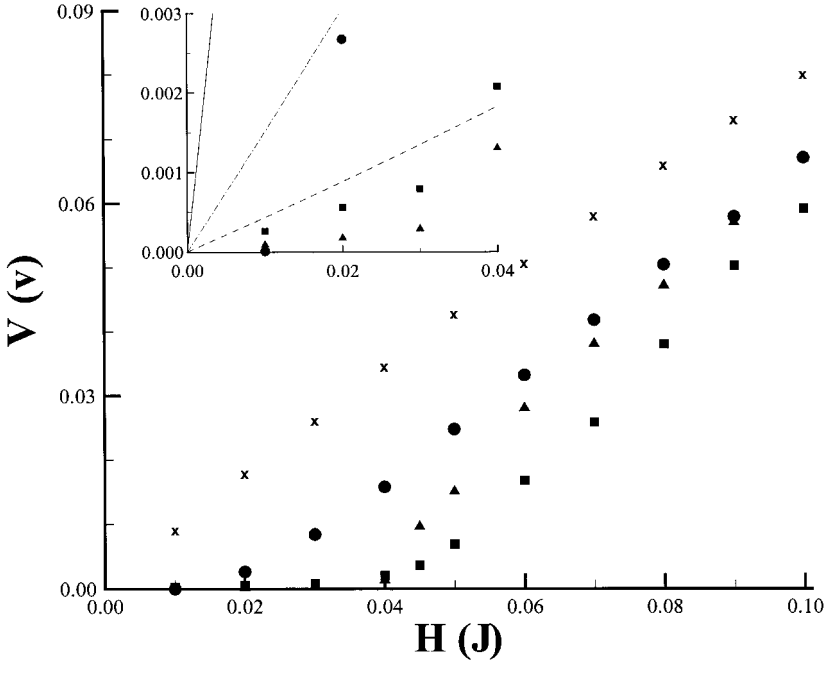

Figure 6. The dependence of the mean boundary velocity V on the driving force for three different diffusivities ((●), $D = 0$; (▲), $D = 0.0229a^2\,(\mathrm{MCS\,site^{-1}})^{-1}$; (■), $D = 0.0916a^2\,(\mathrm{MCS\,site^{-1}})^{-1}$); (×), velocity of the boundary in the absence of impurities. The inset shows an expanded view of the low-velocity portion of the plot. The simulations were performed using $C_\infty = 0.01$ and $T = 0.5\,\mathrm{J}/k$. The lines in the inset are the predictions from Cahn's model under the same conditions as for the simulations ((——), no impurities; (- - - -), $D = 0.0229a^2\,(\mathrm{MCS\,site^{-1}})^{-1}$; (—·—), $D = 0.0916a^2\,(\mathrm{MCS\,site^{-1}})^{-1}$).

pinning impurities. Below the transition in the boundary mobility, the boundary velocity is nearly zero in the $D = 0$ case. Theoretical analyses of boundary migration with diffusing impurities (Cahn 1962) suggested that the origin of impurity drag is associated with the modification of the impurity distribution. When $D = 0$, such impurity redistribution does not occur and there should be no drag. This is clearly inconsistent with the simulation results presented in figure 6 (see discussion below).

Analysis of the continuum theories (for example Cahn (1962)) for the influence of diffusing impurities on boundary migration suggest that changing the sign of the impurity–boundary interaction has no effect (at least for the triangular well and exponential interaction potentials). To investigate this prediction we performed several series of simulations with different interaction strengths E_0, with the same parameters as above (series 1). We used $E_0 = -1.63$ (series 4, i.e. smaller attraction than in series 1) and $E_0 = 1.63$ and $E_0 = 3.26$ (series 5 and 6, i.e. repulsive interactions of the same strength as in series 4 and 1, respectively). The results are shown in figure 7. This figure demonstrates that the impurity drag effect strongly depends on the sign of the impurity–boundary interaction. At least at low velocities, repulsive impurities have less of an influence on boundary migration than do attractive impurities. Instantaneous configurations corresponding to series 1 and 6 (opposite interaction sign) are shown in figure 2. Comparison of these configurations shows that, at the same small driving force, the perturbation of the impurity distribution by the boundary is much greater in the attractive case. Figure 2 also shows that the boundary roughness is considerably greater when the impurity–boundary interactions are

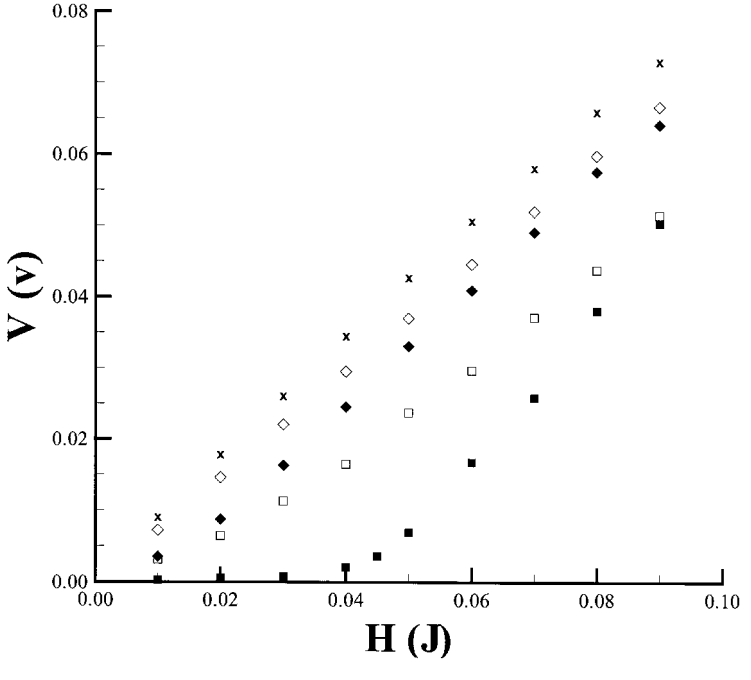

Figure 7. The dependence of the mean boundary velocity V on the driving force for four different interaction strengths ((□), (■), $|E_0| = 3.26$; (◇), (◆), $|E_0| = 1.63$; (□), (◇), positive interactions; (■), (◆), negative interactions): (×), velocity of the boundary in the absence of impurities. The simulations were performed using $C_\infty = 0.01$, $D = 0.0916a^2\,(\mathrm{MCS\,site^{-1}})^{-1}$ and $T = 0.5\,\mathrm{J}/k$.

attractive. This is quantified in figure 5 (*a*), where the excess boundary length (roughness) in the attractive case is seen to be considerably larger than in the repulsive case. However, at larger driving forces, the differences in the impurity distribution are small. At small driving forces, both the roughness and the slope of the velocity–driving force plot (figures 5 (*a*) and 7) for $E_0 = 3.26$ undergo a transition at a driving force H of 0.03.

To investigate the influence of the temperature on grain-boundary migration we performed additional simulations at $T = 0.25\,\mathrm{J}/k$ (the previous simulations were at $T = 0.50\,\mathrm{J}/k$). In nature, the temperature effects both the magnitude of thermal fluctuations as well as the magnitude of the diffusivity. Commonly, it is the temperature dependence of the diffusivity that has the largest effect. In order to separate these two effects, we first performed simulations (series 7 and 8 corresponding to attractive and repulsive impurity–boundary interactions respectively) in which the temperature was changed, but where the diffusivity was fixed. Comparison of the low-temperature (figure 8) and high-temperature (figure 7) results for the same interaction strength shows several interesting features. First, the overall velocity for a given driving force is considerably lower at low temperature. This demonstrates that boundary migration, even in the absence of impurities, is thermally activated (Mendelev and Srolovitz 2000a). Second, there is a much more abrupt transition from the low- to the high-velocity branch at low temperatures than at high tempera-

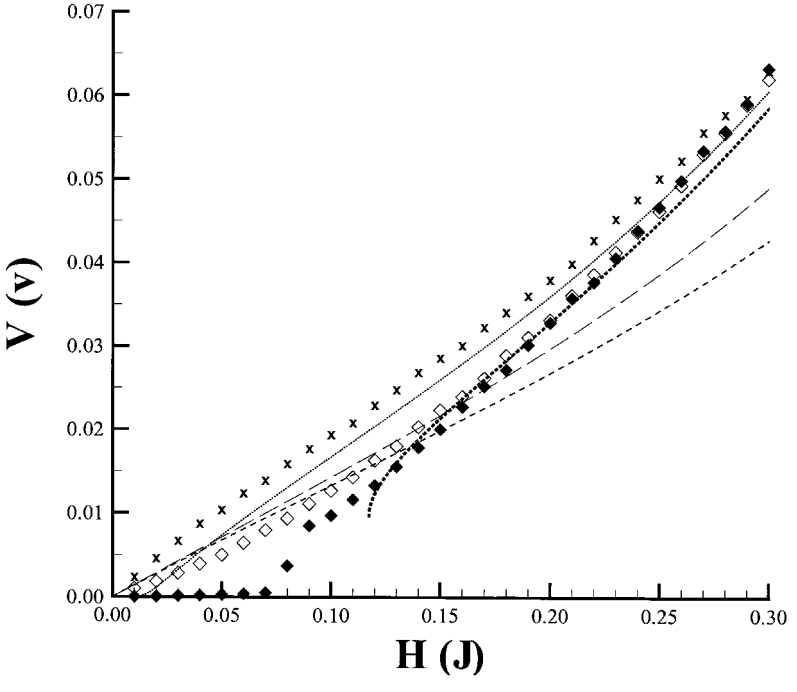

Figure 8. The dependence of the mean boundary velocity V on the driving force for impurities with $E_0 = -1.63\,\mathrm{J}$ (◆) and $E_0 = 1.63\,\mathrm{J}$ (◇): (×), velocity of the boundary in the absence of impurities. The simulations were performed using $C_\infty = 0.01$, $D = 0.0916a^2\,(\mathrm{MCS\,site}^{-1})^{-1}$ and $T = 0.25\,\mathrm{J}/k$. The results for Cahn's model with (— — —) and without (- - - -) corrections for site saturation and for the discrete model with $E_0 = 1.63\,\mathrm{J}$ (· · · · ·) and $E_0 = -1.63\,\mathrm{J}$ (· · · · ·) are also shown.

tures, for the case of attractive impurities. On the other hand, when the impurities are repelled from the boundary, the low- and high-temperature data are much more similar. Figure 9 shows the results of a series of simulations where both the temperature and the diffusivity were changed simultaneously (series 9 and 10), for the case where the activation energy for diffusion is large ($D = 0.00168$ at $T = 0.25\,\mathrm{J}/k$, and $D = 0.0916$ at $T = 0.50\,\mathrm{J}/k$). Comparison of figures 8 and 9 shows that decreasing the diffusivity decreases the transition driving force between the small- and large-driving-force behaviours. This is consistent with the results shown in figure 6 at a higher temperature. We consider this case in more detail below, when we examine the predictions of the theoretical models.

As noted above, most of the theoretical models assume that the impurities are in ideal solution within the matrix. In all the simulations reported to this point, the solid solution is non-ideal because the impurities repel one another ($\phi = 1$). In order to gauge the effects of this non-ideality, we performed additional simulations in the ideal limit (series 11 and 12), where there is no interaction between impurities ($\phi = 0$). The results, presented in figure 9, clearly demonstrate that at least under the conditions of these simulations, the effects of non-ideality are negligible.

The effects of changing impurity concentration are shown in figure 10 for $C_\infty = 0.001$ (series 13 and 14) and $C_\infty = 0.005$ (series 15 and 16). Not too surpris-

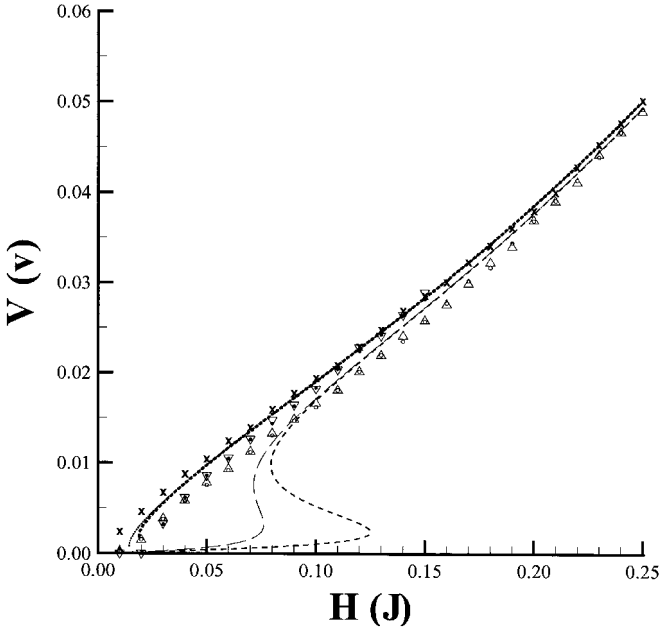

Figure 9. The dependence of the mean boundary velocity V on the driving force for interacting and non-interacting impurities: (×), velocity of the boundary in the absence of impurities. (△), data corresponding to interacting impurities ($\phi = 1$) and $E_0 = -1.63\,\mathrm{J}$; (▽), data corresponding to interacting impurities ($\phi = 1$) and $E_0 = -1.63\,\mathrm{J}$; (●), data corresponding to non-interacting impurities ($\phi = 1$) and $E_0 = -1.63\,\mathrm{J}$; (○), data corresponding to non-interacting impurities ($\phi = 0$) and $E_0 = 1.63\,\mathrm{J}$. The simulations were performed using $D = 0.00168a^2\,(\mathrm{MCS\,site}^{-1})^{-1}$, $C_\infty = 0.01$, and $T = 0.25\,\mathrm{J}/k$. The results for Cahn's model with (— — —) and without (- - - -) corrections for site saturation, and for the discrete model with $E_0 = 1.63\,\mathrm{J}$ (· · · · ·) and $E_0 = -1.63\,\mathrm{J}$ (· · · ·) are also shown.

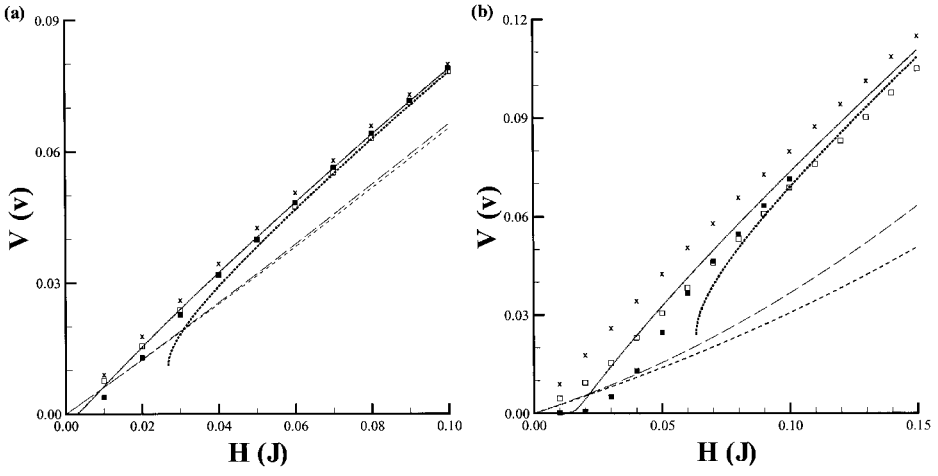

Figure 10. The dependence of the mean boundary velocity V on the driving force for impurities with $E_0 = -3.26\,\mathrm{J}$ (■) and $E_0 = 3.26\,\mathrm{J}$ (□) for two different solute concentrations (*a*) $C_\infty = 0.001$ and (*b*) $C_\infty = 0.005$: (×), velocity of the boundary in the absence of impurities. The simulations were performed using $D = 0.091a^2\,(\mathrm{MCS\,site^{-1}})^{-1}$ and $T = 0.5\,\mathrm{J}/k$. The results for Cahn's model with (— — —) and without (- - - - -) corrections for site saturation, and for the discrete model with $E_0 = 3.26\,\mathrm{J}$ (· · · · ·) and $E_0 = -3.26\,\mathrm{J}$ (· · · · ·) are also shown.

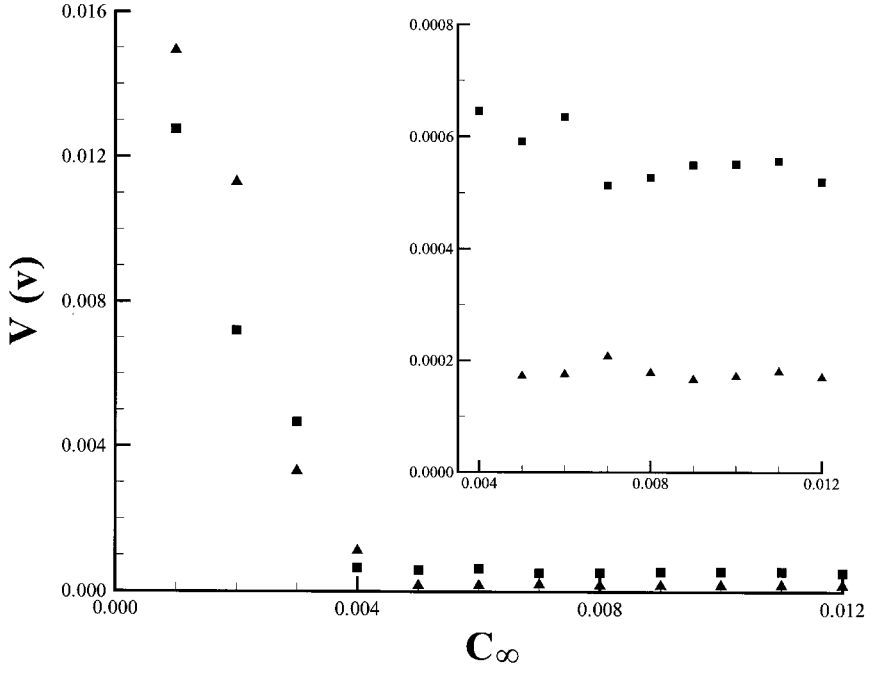

Figure 11. The dependence of the mean boundary velocity V on the impurity concentration C_∞ for two different diffusivities ((■) $D = 0.0916a^2\,/(\mathrm{MCS\,site^{-1}})^{-1}$; (▲), $D = 0.0229a^2\,(\mathrm{MCS\,site^{-1}})^{-1}$). These simulations were performed at fixed $H = 0.020\,\mathrm{J}$, $E_0 = -3.26$ and $T = 0.5\,\mathrm{J}/k$. The inset shows an enlargement of this figure at low velocities.

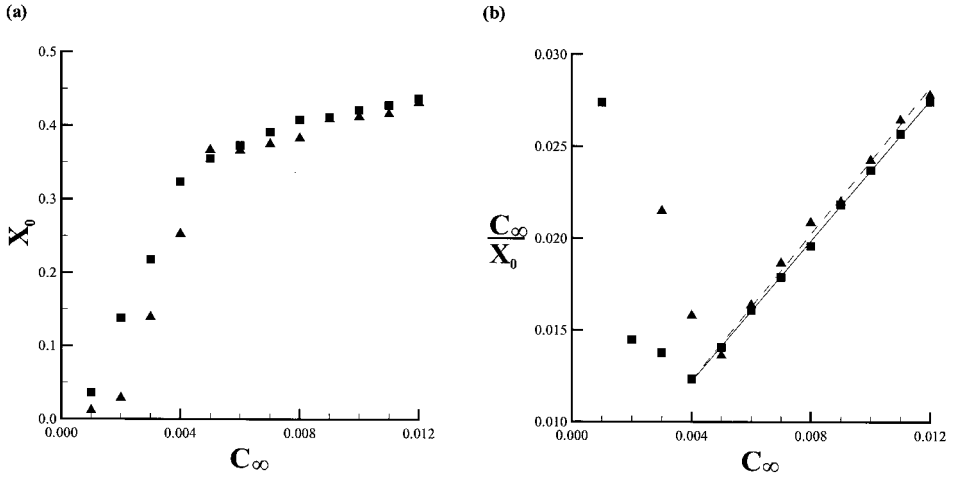

Figure 12. The impurity concentration at the boundary versus bulk impurity concentration on (*a*) linear scale and (*b*) in a form convenient for comparison with the Langmuir segregation isotherm for the same conditions as in figure 11: (——), linear fit to the data for $C_\infty \geqslant 0.005$ for $D = 0.0229a^2\,(\mathrm{MCS\,site^{-1}})^{-1}$; (– – –), linear fit to the data for $C_\infty \geqslant 0.005$ for $D = 0.0916a^2\,(\mathrm{MCS\,site^{-1}})^{-1}$.

ingly, lowering the bulk impurity concentration decreases the driving force required for the transition between the small- and large-driving-force behaviours (cf. figures 7 and 10). The effect of impurity concentration on boundary velocity at a fixed driving force is shown in figure 11. Two distinct regimes are seen. In the low-concentration regime, the boundary velocity drops precipitously with increasing impurity concentration while, at the higher (although still low) concentrations, the boundary velocity is nearly independent of bulk impurity concentration (see the inset of figure 11). In order to understand this transition, we examined the variations in the impurity concentration (X_0) at the boundary with bulk impurity concentration (figure 12(*a*)). While increasing the bulk impurity concentration leads to an increase in the impurity concentration at the boundary, there is no abrupt change at the bulk concentration where the velocity shows an abrupt change in behaviour at $C_\infty \approx 0.05$ in figure 11. It is interesting to compare this boundary concentration dependence on bulk concentration with that predicted for Langmuir segregation $X_0 = X_s bC_\infty/(1 + bC_\infty)$, where X_s is the saturated boundary concentration and b is a constant depending only on the temperature. In order to determine how well the Langmuir isotherm fits the data in figure 12(*a*), we plot C_∞/X_0 versus C_∞, which should be a straight line of slope $1/X_s$ if the Langmuir isotherm pertains (see figure 12(*b*)). This figure shows that the Langmuir isotherm describes boundary segregation only in the high-bulk-concentration region. This region ($C_\infty > 0.05$) corresponds to the concentration regime where the velocity is low (and is independent of the bulk concentration; see figure 11).

§4. Analytical models for boundary migration

4.1. *Comparison with continuum model*

We now compare the simulation results with the predictions of Cahn's (1962) continuum model for the influence of diffusing impurities on boundary migration.

One of the parameters in this model is the impurity–boundary interaction profile $E(x)$. If the boundary is perfectly flat, then the impurity–boundary interaction energy within the simulation model is (equation (13))

$$E(x) = \begin{cases} E_0, & x = 0, \\ 0, & |x| \geqslant a, \end{cases}$$

where a is the lattice parameter. In the theoretical analyses, we model these interactions as a triangular potential, like that considered in detail by Cahn (1962):

$$E(x) = \begin{cases} E_0 + \dfrac{E_0}{a}x, & x \leqslant 0, \\ E_0 - \dfrac{E_0}{a}x, & x \geqslant 0. \end{cases} \tag{16}$$

In this case, the differential equation (equation (6)) describing the concentration profile may be easily solved (Cahn 1962). Inserting this concentration profile into equations (7) and (8) allows us to determine the velocity–driving force relation for Cahn's model. Figure 13 shows the predicted form of this relation for the cases simulated in series 1, 2 and 6. For the triangular interaction potential, this velocity–driving force relation is independent of the sign of E_0. This is clearly inconsistent with the simulation results presented above (see for example figure 7). This implies that the continuum model is unable to describe the simulation results even qualitatively.

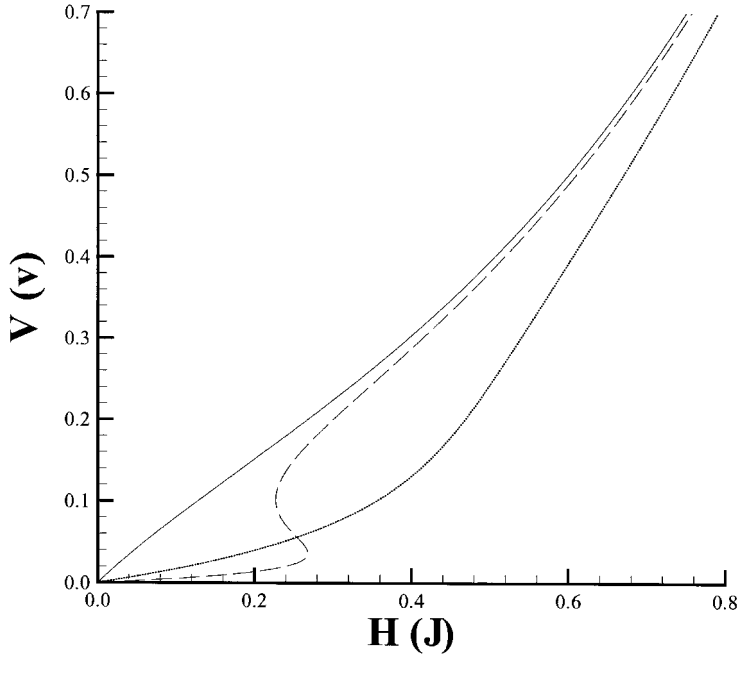

Figure 13. The boundary velocity versus driving force without impurities (——) and according to Cahn's model for $D = 0.0229a^2\,(\text{MCS site}^{-1})^{-1}$ (– – – –) and $D = 0.0916a^2\,(\text{MCS site}^{-1})^{-1}$ (· · · · ·). These calculations were made assuming that $E_0 = -3.26, C_\infty = 0.01$ and $T = 0.5\,\text{J}/k$.

Figure 13 shows that, under some conditions, the curve of the theoretical velocity versus the driving force is multivalued. This implies a jump in velocity at two different driving forces, depending on whether the driving force is being increased or decreased, leading to hysteresis (Lücke and Stüwe 1971). This sudden jump in velocity upon changing driving force is never observed in the present simulations.

The continuum model predicts a jump from a low-velocity to a high-velocity regime over the range $H = 0.23$–0.27, for $D = 0.0229$ (figure 13). While we have no simulation data for $H > 0.1$, the simulations results in figure 6 (*a*) show both a low- and a high-velocity regime at a much smaller driving forces (near $H = 0.04$). Examination of the simulation results for $D = 0.0916$ (figure 6 (*a*)), shows a similar, relatively sharp transition from a low- to a high-velocity regime. No such sharp transition is predicted by the theory in this case. Figure 9 shows a case where both the theory and the simulations exhibit well defined transitions from low- to high-velocity regimes, but where the transitions occur at driving forces which differ by a factor in excess of 6.

For the case shown in figure 8, the continuum model predicts no transitions; however, they clearly exist in the simulation data (especially for the attraction case). For the case shown in figure 9, there are transitions both in the simulations and in the theory. The driving force where this transition occur is poorly predicted by the continuum model.

There are several possible reasons why the theoretical model neither quantitatively nor qualitatively describe the simulations results. These deficiencies were pointed out in the introduction. We now examine whether these deficiencies account for the disagreement between theory and simulation.

4.2. *Site saturation at the boundary*

One of the deficiencies in the continuum model (Cahn 1962) described above was that it does not account for the fact that there are only a limited number of sites at the boundary (i.e. site exclusion or saturation). For example, for the case when $E_0 = -3.26$, used often in the simulations, the equilibrium concentration at the boundary predicted by equation (1) is $X_0 = X_\infty \exp(-E_0/kT) = 6.79$, where $X_\infty = C_\infty/(1 - C_\infty)$. X_0 must, of course, be less than or equal to unity; hence, analyses that do not account for site saturation are clearly inapplicable when equation (1) predicts $X_0 > 1$. Lücke and Stüwe (1963), recognizing this problem, corrected the diffusion equation for the case of the moving boundary (equation (9)). We can rewrite equation (9), accounting for the fact that the maximum impurity concentration X_s at the boundary is less than or equal to unity:

$$D\frac{\mathrm{d}X}{\mathrm{d}x} + \frac{D}{kT}\frac{X(X_s - X)}{X_s}\frac{\mathrm{d}E}{\mathrm{d}x} + VX = VX_\infty, \tag{17}$$

where the fraction X of impurity sites occupied by impurities is a function of the spatial coordinate x. Equation (17) is valid provided that the maximum impurity interstitial site concentration X_s is the same at the boundary and in the bulk. Mathematically, equation (17) is the Riccati equation and is easily solved for a triangular potential. In the present simulations, the impurities repel each other (except for series 12), effectively preventing impurities from occupying adjacent sites (i.e. $X_s = 1/2$ rather than 1, consistent with figures 5 (*b*) and 12).

Following Cahn (1962), we determine the velocity–force relationship taking into account site saturation using the concentration profile from equation (17). We do

this by inserting the resultant impurity concentration profile into the equation for the drag force (equation (7) with X replacing C), substituting this drag force into equation (8) and solving for the velocity. The resultant velocity–force relationship is independent of the sign of E_0, as in Cahn's original theory.

Figure 14 shows a comparison of Cahn's theory with that corrected for site saturation and the simulation results (series 1 and 6). The difference between the two theoretical curves is relatively small. Accounting for site saturation decreases the impurity concentration on the boundary, thereby reducing the impurity drag effect. The effects of site saturation should become even less important as the degree of segregation decreases. This is confirmed where the decrease in segregation comes from decreases in the magnitude of E_0/kT (cf. figures 14 and 15 and figures 8 and 15) and for lower bulk impurity concentrations (cf. figures 10 and 14). In cases where the theory shows a jump in the velocity (i.e. where the velocity–driving force profile is multivalued; see figure 9), large differences between the theories with and without site saturation are observed near the jump. On the other hand, far from the jump (i.e. low and high velocities) the theories with and without site saturation show only small differences. Taking site saturation into account shifts the jump towards smaller driving forces. In all the velocity–driving force curves shown, inclusion of the site saturation effect does little to improve the generally poor agreement between the simulations and the theory.

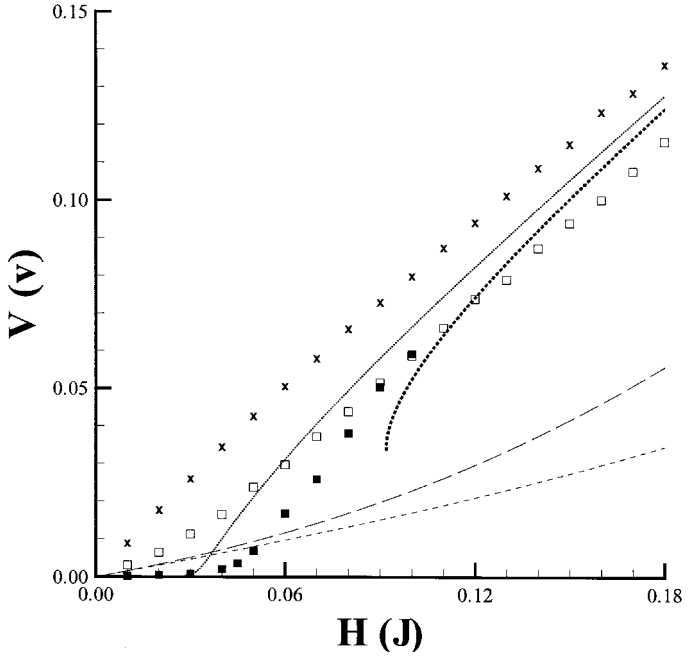

Figure 14. The dependence of the mean boundary velocity V on the driving force for impurities with $E_0 = -3.26\,\mathrm{J}$ (■) and $E_0 = 3.26\,\mathrm{J}$ (□): (×), velocity of the boundary in the absence of impurities. The simulations were performed using $C_\infty = 0.01$, $D = 0.0916a^2\,(\mathrm{MCS\,site^{-1}})^{-1}$ and $T = 0.5\,\mathrm{J}/k$. The results for Cahn's model with (— — —) and without (- - - - -) corrections for site saturation and for the discrete model with $E_0 = 3.26\,\mathrm{J}$ (· · · · ·) and $E_0 = -3.26\,\mathrm{J}$ (· · · · ·) are also shown.

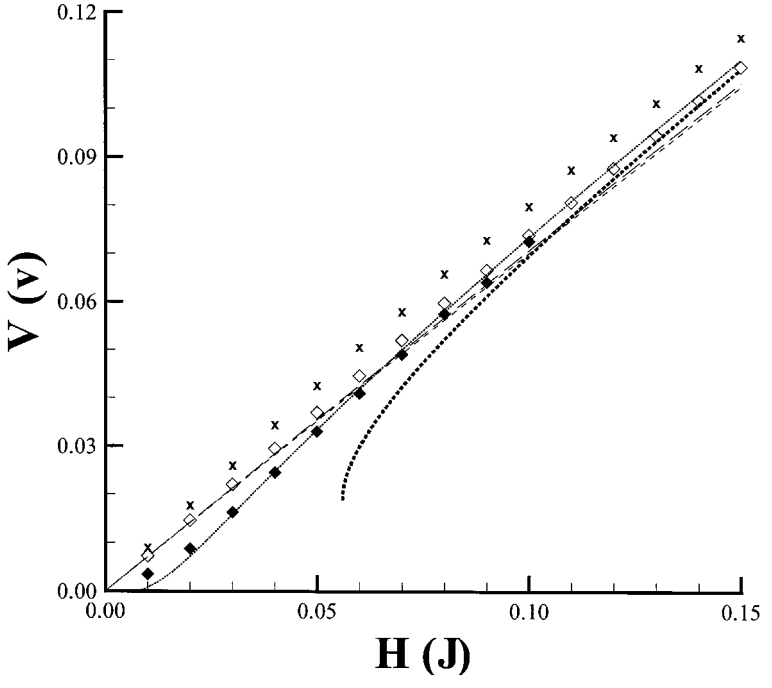

Figure 15. The dependence of the mean boundary velocity V on the driving force for impurities with $E_0 = -1.63\,\mathrm{J}$ (◆) and $E_0 = 1.63\,\mathrm{J}$ (◇): (×), velocity of the boundary in the absence of impurities. The simulations were performed using $C_\infty = 0.01$, $D = 0.0916a^2\,(\mathrm{MCS\,site^{-1}})^{-1}$ and $T = 0.5\,\mathrm{J}/k$. The results for Cahn's model with (— — —) and without (- - - - -) corrections for site saturation and for the discrete model with $E_0 = 1.63\,\mathrm{J}$ (· · · · ·) and $E_0 = -1.63\,\mathrm{J}$ (· · · · ·) are also shown.

4.3. *Discrete model*

Another important difference between the theoretical models and the simulations (and any real system) revolves around the continuum descriptions of impurities and boundaries in the theory and the inherent discreteness of atomic systems. This difference was pointed out by Lücke and Stüwe (1971). We now develop a model that includes the discreteness of the impurity distribution and site saturation.

Consider the description of the system and notation shown in figure 16 for the case where impurities are attracted to the boundary ($\Delta E < 0$). For impurities that are not near the boundary (i.e. at $|i| \geqslant 1$), the flux $J_{i+1/2}$ across a solute atom plane is simply the difference between the forward and backward fluxes:

$$\begin{aligned} J_{i+1/2} &= J^{\rightarrow}_{i+1/2} - J_{i+1/2} \\ &= \frac{aM}{4} n X_i \frac{X_s - X_{i+1}}{X_s} - \frac{aM}{4} n X_{i+1} \frac{X_s - X_i}{X_s} \\ &= \frac{aM}{4} n (X_i - X_{i+1}) \\ &= -\frac{D}{a} n (X_{i+1} - X_i), \end{aligned} \tag{18}$$

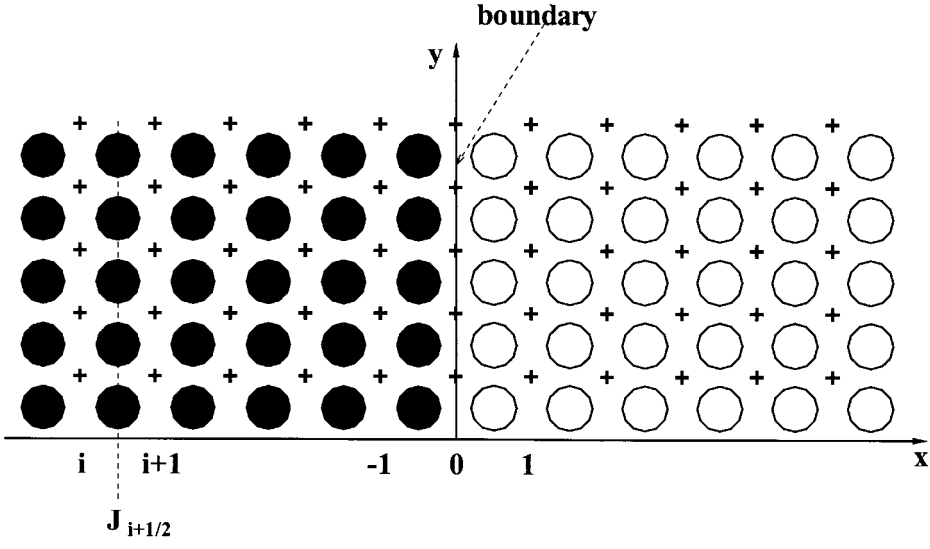

Figure 16. A schematic illustration of the discrete model discussed in the text, indicating the labelling of solute and impurity planes and the boundary position.

where M is the impurity jump attempt frequency, a is the distance between atomic planes and the diffusivity $D = a^2M/4$. Analogously for $J_{-1/2}$ we obtain

$$\begin{aligned} J_{-1/2} &= \vec{J_{-1/2}} - J_{-1/2} \\ &= -\frac{D}{a}n(X_0 - X_{-1}) + \frac{D}{a}n\frac{X_0(X_x - X_{-1})}{X_s}\left[1 - \exp\left(\frac{\Delta E}{kT}\right)\right], \end{aligned} \tag{19}$$

where the factor $\exp(\Delta E/kT)$ arises because of the difference between the energies of an impurity on a boundary site and an impurity on a non-boundary site. Finally, for $J_{1/2}$ we obtain

$$\begin{aligned} J_{1/2} &= \vec{J_{1/2}} - J_{1/2} \\ &= -\frac{D}{a}n(X_1 - X_0) - \frac{D}{a}n\frac{X_0(X_s - X_1)}{X_s}\left[1 - \exp\left(\frac{\Delta E}{kT}\right)\right]. \end{aligned} \tag{20}$$

When the boundary is moving with the steady-state velocity V, the impurity flux in the moving frame is (cf. equations (5) and (6))

$$J_{i+1/2} - nX_{i+1}V = -nX_\infty V. \tag{21}$$

Substituting equations (18)–(20) into this flux equation yields

$$X_i = \begin{cases} \dfrac{VX_\infty + (D/a)X_{i-1}}{V + D/a} = X_\infty, & i < 0, \\ \dfrac{(V + D/a)X_\infty}{V + D/a - (D/a)[(X_s - X_\infty)/X_s][1 - \exp(\Delta E/kT)]}, & i = 0, \\ \dfrac{VX_\infty + (D/a)X_0 \exp(\Delta E/kT)}{V + D/a - (D/a)(X_0/X_s)[1 - \exp(\Delta E/kT)]}, & i = 1. \end{cases} \tag{22}$$

If $V = 0$, we obtain $X_0 = [X_\infty X_s \exp(-\Delta E/kT)]/[X_s - X_\infty + X_\infty \exp(-\Delta E/kT)]$ and $X_1 = X_\infty$. This is consistent with the continuum solution (cf. equation (10)).

If the boundary moves by one interatomic distance to the right, only the energies of the impurities in layers 0 and 1 change. Therefore the impurity drag force is simply

$$P_i = -\frac{\Delta E}{a}(X_0 - X_1)na. \tag{23}$$

The driving force required to move the boundary with the steady-state velocity V has contributions from the intrinsic drag force (i.e. that needed to move it in the absence of impurities (Mendelev and Srolovitz 2000a)) and the drag force (see equation (8)). The dependence of this driving force on the velocity is shown in figure 17 for series 1 (for our simulation, $P = 2H/a$). This plot shows that there is no solution for small driving forces $H < H^*$. Therefore, for $H < H^*$ the boundary does not move ($V = 0$) even though $H > 0$. The large-H small-V ($V < V^*$) branch is unstable and we shall not consider it.

Comparisons of the discrete model with the simulation data may be found in figures 8–10, 14 and 15 for a variety of cases. Overall, these comparisons show much better agreement between the simulations and the discrete model than between the simulation and Cahn's original model (or that with site saturation). Figure 9 shows that the discrete model predicts a transition between the high- and low-velocity regimes in very good agreement with the simulation. (Note, that the low-velocity regime corresponds to $V = 0$ in this model, i.e. this is a model only for the high-velocity regime.) While the continuum model also predicts a transition, this prediction is in poor agreement with the simulations. For the cases shown in figures 8, 10,

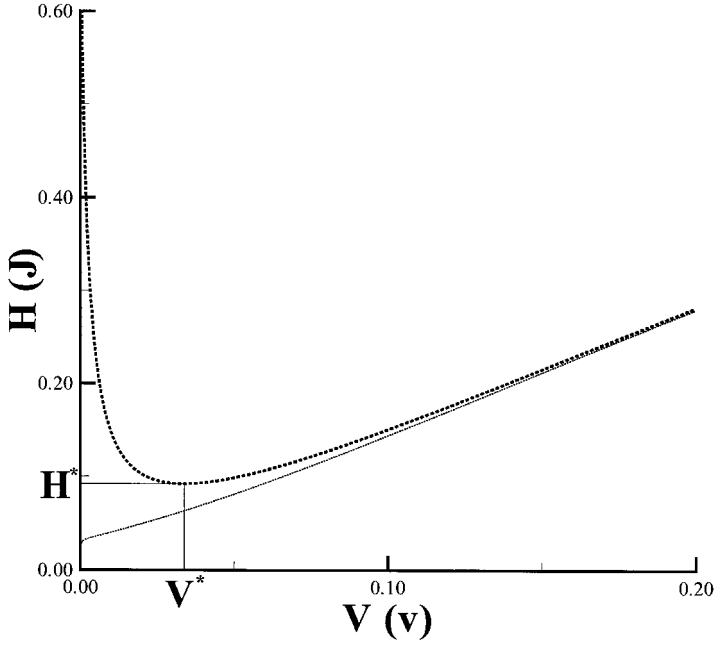

Figure 17. A plot of the impurity drag force as a function of the boundary velocity for the discrete model for $E_0 = -3.26$ ($\cdots\cdots$) and $E_0 = 3.26$ ($\cdots\cdots$). These calculations were made assuming that $D = 0.0916a^2\,(\text{MCS site}^{-1})^{-1}$, $C_\infty = 0.01$ and $T = 0.5\,\text{J}/k$.

14 and 15, the simulations and the discrete model all exhibit transitions, while the continuum model does not. Nonetheless, the discrete model often predicts the driving force at which the transition will occur in excess of that seen in the simulations. The observation that the boundary is able to move at driving forces smaller than the predicted threshold is attributable to two effects: thermal fluctuations and the fact that the boundary is not flat. Since the impurity concentration is not uniform along the entire boundary, some segments of the boundary see locally enhanced concentrations while other segments see low concentrations. Near the threshold, this implies that some segments of the boundary will be above the threshold and others below. Therefore, above the threshold for the entire boundary (predicted using the discrete model), some segments of the boundary are able to move. Once one segment moves, regions of large curvature develop near the end of the moving segment, which aids the escape of the pinned segment from its impurity cloud.

We now consider the case where the impurities are repelled from the boundary ($\Delta E > 0$). Following the same procedure that led to equation (22), we find that

$$X_i = \begin{cases} \dfrac{VX_\infty + (D/a)X_{i-1}}{V + D/a} = X_\infty, & i < 0, \\ \dfrac{[V + (D/a)\exp(-\Delta E/kT)]X_\infty}{V + D/a - (D/a)(X_\infty/X_s)[1 - \exp(-\Delta E/kT)]}, & i = 0, \\ \dfrac{VX_\infty + (D/a)X_0}{V + D/a - (D/a)[(X_s - X_0)/X_s][1 - \exp(-\Delta E/kT)]}, & i = 1. \end{cases} \tag{24}$$

If $V = 0$, we obtain the same static solution as above. The relationship between the driving force and the velocity for the repulsive impurity–boundary interaction is very different from the case where this interaction is attractive, as shown in figure 17. As in the attractive case ($\Delta E < 0$), there is no solution (i.e. the velocity is zero) in the repulsive case ($\Delta E > 0$) for $H < H^*$. The two solutions differ in that in the repulsive case there is only a single branch on the H versus V curve, while there are two in the attractive case. This implies that, in the repulsive case, there should be no jump in velocity. The fact that the driving force–velocity relations are different for the attractive and repulsive cases is a feature of the discrete model not seen in the continuum theories. Examination of the simulation results shows that this effect is real and large.

The discrete model predicts that the transition between the two regimes of boundary motion occurs at a smaller driving force for the case of repulsive impurities than for attractive impurities (of the same $|E_0|$). This is consistent with the simulation data shown in figures 8–10, 14 and 15. For high $|E_0|$, the agreement between the discrete model and the simulation results is considerably better than between the continuum models and the simulation (see figures 10 and 14). Nonetheless, the agreement is not perfect. The discrete model works very well at low concentrations (see figure 10). However, for the cases shown in figure 10(*a*), the effect of the impurities on the velocity–force relationship is minimal. At low temperatures, the agreement between the discrete model and the simulation results is satisfactory in the case of attractive interactions and less accurate in the repulsive case (see figures 8 and 9). Even so, the exact point of the transition is not always accurately reproduced (see figure 8), as discussed below. The deviation in the discrete model predictions from the simulation data cannot be attributed to the solution thermodynamics (figure 9 shows data for both ideal and non-ideal solutions).

4.4. *Zero diffusivity*

Finally, we consider the influence of impurities on boundary migration in the limit of zero impurity diffusivity, $D = 0$. The analytical models (both continuum and discrete) predict zero impurity drag for $D = 0$. Hence, in this limit, the impurities do not modify the velocity–force curve of the pure system. Examination of figure 6 shows that this is not true. The failure of the analytical models is a result of the fact that they are one dimensional, that is the boundary is flat. A flat boundary necessarily has an impurity concentration equal to X_∞ at $D = 0$. The real boundary, on the other hand, is free to deform to maximize (attractive case) or to minimize (repulsive case) the impurity content of the boundary (subject to surface tension restrictions). Figure 5 (*b*) shows that, even in the case when $H = 0$, the impurity content of the boundary is $X_0 = 0.08$, that is eight times the average concentration. X_0 increases with increasing H, reaching a maximum, and then decreases very slowly at large H. The increase in X_0 at small H is associated with the boundary becoming locally pinned at locations where the impurity concentration is stochastically larger than average. If we assume that X_0 does not depend on H (a good approximation for $D = 0$; see figure 5 (*b*)), the driving force can be written as

$$P = P_0(V) + nE_0X_0. \tag{25}$$

Since $P_0(0) = 0$, the minimal field required to move the boundary is

$$P^* = nE_0X_0. \tag{26}$$

For the case shown in figure 6 (*a*), equation (26) predicts that $H^* = 0.13$. This is in reasonable agreement with the simulation results (figure 6 (*a*)). Equation (25) shows that, in the $D = 0$ case, the velocity–force curves for pure systems and those with impurities are parallel. This is also consistent with the simulation data shown in figure 6 (*a*).

§ 5. Discussion and Conclusions

A critical comparison of analytical models for the motion of grain boundaries in the presence of diffusing impurities with experimental data is difficult to make because the strengths of the impurity–boundary interactions (and other properties) are generally unknown. Moreover, if theory and experiment differ, it is difficult to determine the origin of this difference (e.g. assumptions about the ideality of the solid solution or errors in determining the parameters that go into the theory). Computer simulation provides a systematic approach to control precisely the fundamental physical parameters and assumptions in order to assess the reliability of the theoretical analyses.

The simulation results, presented above, clearly show that the classical continuum models are unsuitable for describing boundary motion in the presence of impurities. There are three main reasons for the failure of these models.

(i) Real systems are discrete, while the models are continuous.
(ii) Real boundaries are not flat, although the models impose this constraint (i.e. they are one dimensional).
(iii) Impurities modify the boundary migration mechanism by altering kink formation and propagation, while this level of atomistic realism is absent in the models.

The discrete revision of the classical model suggested in the present work *does not* account for the real (discrete) shape of the boundary and the mechanism of its motion. The discrete model predicts that the boundary is completely pinned by impurities at small driving forces, moves at large driving forces and has an abrupt transition between these at a finite driving force. *This discrete model is clearly inapplicable in the small driving force regime.*

One of the most obvious failures of the continuum models is the prediction that the sign of the impurity–boundary interaction has no influence on the boundary velocity, in sharp distinction to the simulation results. On the other hand, the discrete model presented here is able to capture the fundamental difference between attractive and repulsive impurities. The discrete model shows that the magnitude of the impurity drag is determined by the difference between the impurity concentration at the boundary and in the layer ahead of the boundary (see equation (23)). This is in contrast with the continuum models, where the impurity drag is determined by an integral over the entire concentration profile (from $-\infty$ to $+\infty$). When the boundary velocity is low and the impurity–boundary interactions are strong, the impurity concentration is $X_0 = X_s$ for attractive interactions, $X_0 = 0$ for repulsive interaction and $X_1 = X_\infty$ for both cases. Since $|X_s - X_\infty| \gg |X_0 - X_\infty|$ at low velocities, the impurity drag effect at low velocities is much larger in the attractive case than in the repulsive case. Moreover, the discrete model presented here also shows that the transition between the low- and high-velocity regimes occurs at a smaller value of the driving force in the repulsive case than in the attractive case. Both of these predictions are consistent with the simulation results (see figures 8–10, 14 and 15).

We now compare the discrete model proposed in the present work with the early discrete model developed by Lücke and Stüwe (1971). While this early model employs a different form of the impurity–boundary interaction from that considered here (in addition, their boundary is twice the thickness of ours), it is a simple matter to reconsider it within the framework of the present type of impurity–boundary interaction. Therefore, we can compare the general concepts and results. The two models employ the same approach to determine the impurity concentration near the boundary (except that we additionally take into account site saturation). The main difference between the discrete models is the method by which the impurity drag effect is determined. We consider a flat boundary, while Lücke and Stüwe considered the jumps of individual atoms at the boundary. Therefore, the boundary in the Lücke–Stüwe model is not flat. Since the hops of the individual atoms are uncorrelated, their boundary does not move by the formation and propagation of kinks, but rather as a boundary with zero surface (boundary) tension. Nonetheless, the remainder of the model is based on the (inconsistent) assertion that this is a one-dimensional problem. On the other hand, in our discrete model (presented above), we make the opposite assumption; that is the surface tension is infinite such that the boundary remains flat (consistent with the one-dimensional assumption). The reason that the boundary velocity is finite at very small driving forces in the Lücke–Stüwe model is that they allow different sections (of atomic dimensions). While motion at small driving forces is a desirable feature, it is a result of inconsistency in their model and hence cannot be viewed as yielding reliable predictions. On the other hand, the discrete model that we present is not applicable at all in this small-driving-force limit. Nevertheless, we believe that our model is preferable. First, our assumption is consistent with the analysis of the concentration profile around the boundary (i.e. equation (21)) that both we and

Lücke and Stüwe use (i.e. it assumes a flat boundary). Second, although the present discrete model is incapable of predicting the small-driving-force behaviour, it does predict a transition to the high velocity behaviour at a point which is in much better agreement with the simulations than the continuum model (Lücke and Stüwe claimed that their results are equivalent to the same continuum model). Finally, the present discrete model predicts that the transition between the small- and large-driving-force regimes are different for impurities that are attracted and repelled from the boundary, while both the continuum and the Lücke–Stüwe models give exactly the same result for both types of interaction. This is in clear contradiction to the simulation results. The extremely large difference between the attractive and repulsive cases seen in the simulations further suggests that neither the continuum or the Lücke–Stüwe models appropriately describe the small-driving-force regime.

Although no accurate analytical models exist for the small-driving-force regime, the simulations point to several features that could be useful in deriving such a theory. First, boundary segregation in this regime is well described by the Langmuir isotherm. This suggests that, within this regime, the impurities are in equilibrium with respect to the boundary. Second, the boundary velocity is independent of C_∞, provided that the boundary is nearly saturated (as expected at low velocities and temperatures significantly smaller than E_0/k). Finally, the simulation results suggest that in the small-driving-force regime, the boundary mobility is an increasing function of the impurity diffusivity.

When the interaction between the impurities and boundary is strongly attractive, the impurity segregation to the boundary can be appreciable. It is in this case that the influence of the impurities on kink formation and propagation is extremely important. In other words, in these cases, it is inappropriate to consider the boundary motion as simply intrinsic boundary motion with an additional drag from impurities. It is difficult to propose a general model that incorporates the effects of impurities on the boundary migration mechanism as a valid analysis necessarily includes a detailed description of the atomic structure of the boundary and of how it moves. For the particular simulation model used here, the nucleation of a kink–antikink pair on a flat segment of a boundary is larger by a factor of $-2E_0$ when an impurity is at the nucleation site. Since the rate of formation of kink–antikink pairs is a key factor in determining the boundary velocity (Mendelev and Srolovitz 2000a), an increase in the barrier to kink production decreases the boundary velocity. Similarly, an impurity adjacent to a kink raises the barrier for kink propagation. Commonly, the motion of the kink will be limited by the rate at which an impurity atom diffuses away from the kink site (Mendelev and Srolovitz 2000c). This is consistent with the simulation results which show (see inset in figure 6) that the boundary mobility in the low-velocity (i.e. impurity-saturated, figure 5(*b*)) regime increases with increasing impurity diffusivity. The degree to which the impurities slow the boundary motion within the class of Ising models used here depends on the number of nearest neighbours and, hence, the lattice type.

Although the simulation results (see figures 2 and 3) demonstrate that the grain boundaries are not flat, the analytical models implicitly assume that they are (i.e. they are one dimensional). The simulations performed in the zero-diffusivity limit provide a clear demonstration of the importance of boundary roughness. In this limit, the simulations show that there is a threshold driving force for boundary motion (see figure 6). However, if the boundary were strictly flat, the impurity drag effect must be absent. This is a consequence of the fact that for a random

distribution of static impurities there is an equal number of impurities pulling the boundary forwards and backwards such that the total force from impurities is zero (this is also an explicit result from both the continuum and discrete theories). Therefore, the (strong) impurity drag effect in the $D = 0$ case is a consequence of the fact that the boundary is not flat. Examination of images from simulations with $D = 0$ below the transition demonstrates that the bending of the boundary increases the concentration of impurities on the boundary above that expected for a flat boundary. This is confirmed in figure 5(*b*) at $H = 0$ where the concentration of impurities on the boundary is nearly eight times that expected for a flat boundary (i.e. C_∞). This effect of boundary curvature is also present when the diffusivity is non-zero.

The fact that typical boundary configurations are not flat is a consequence of the fact that the spatial distribution of impurities is stochastic. Different segments of the boundary move with different velocities because the impurity drag varies from segment to segment owing to the non-uniform distribution of impurities. This variation in local boundary migration behaviour has a profound influence on the velocity–driving curve in the vicinity of the transition from the low- to high-velocity regimes. Segments with low impurity concentrations move as if they were in the high-velocity regime, while segments where the impurity concentration is locally high move as if they were in the low-velocity regime. Therefore, any jump in velocity at a finite driving force that would occur near the transition in the analytical models is smoothed out by averaging over all boundary segments. The fact that different segments of the boundary can move with different velocities was correctly noted by Cahn (1962). Unfortunately, no analytical models are available that incorporate this variation in local boundary velocities and hence none of the existing models is able to predict properly the velocity–driving force behaviour near the transition between the low- and high-velocity regimes.

Acknowledgements

The authors gratefully acknowledge enlightening discussions with Lasar Shvindlerman and Gunter Gottstein. This work was supported by the Division of Materials Science of the Office of Basic Energy Sciences of the US Department of Energy under grant DE-FG02-99ER45797.

References

Cahn, J. W., 1962, *Acta metallur.*, **10**, 789.

Gottstein, G., and Shvindlerman, L. S., 1999, *Grain Boundary Migration in Metals: Thermodynamics, Kinetics, Applications* (Boca Raton, Florida: CRC Press).

Hillert, M., 1999, *Acta mater.*, **47**, 4481.

Hirth, J. P., and Lothe, J., 1982, *Theory of Dislocations* (New York: Wiley–Interscience).

Lücke, K., and Detert, K., 1957, *Acta metall.*, **5**, 628.

Lücke, K., and Stüwe, H. P., 1963, *Recovery and Recrystallization of Metals*, edited by L. Himmel (New York: Wiley–Interscience), pp. 171–210; 1971, *Acta metall.*, **19**, 1087.

Mendelev, M. I., and Srolovitz, D. J., 2000a, *Acta mater.*, **48**, 3711; 2000b, *ibid.* (in the press); 2000c, *ibid.* (to be published).

Molodov, D. A., Gottstein, G., Heringhaus, F., and Shvindlerman, L. S., 1999, *Mater. Sci. Forum*, **294**, 127.

Mott, N. F., 1948, *Proc. phys. Soc.*, **60**, 391.

Sutton, A. P., and Balluffi, R. W., 1995, *Interfaces in Crystalline Materials* (Oxford: Clarendon).

Westengen, H., and Ryum, N., 1978, *Phil. Mag.* A **38**, 279.